Computer simulation of the tweed microstructure in high-T_c superconductors

1994 J. Phys.: Condens. Matter 6 237

(http://iopscience.iop.org/0953-8984/6/1/022)

J. Phys.: Condens. Matter 6 (1994) 237–252. Printed in the UK

Computer simulation of the tweed microstructure in high-T_c superconductors

K Parlinski†‡ and M Sternik†

† Institute of Nuclear Physics, Ulica Radzikowskiego 152, 31-342 Cracow, Poland
‡ Academic Computer Centre, Cyfronet, Ulica Nawojki 11, Cracow, Poland

Received 28 June 1993

Abstract. The tweed microstructure in the non-stoichiometric crystal of $YBa_2Cu_3O_{7-\delta}$ is studied by computer simulation. A two-dimensional model of 99×99 unit cells represents a layer of this crystal with an oxygen deficit and exhibits a ferroelastic tetragonal–orthorhombic phase transition. The simulation allows us to determine the temperature–oxygen-concentration phase diagram. Below the transition temperature the strain fluctuations form a grid of needle-shaped domains, the density of which increases with increasing degree of non-stoichiometry. On quenching, the tweed texture orders through the intermediate stripe phase, to a single orthorhombic domain. Oxygen vacancies, appearing due to non-stoichiometric oxygen concentration, gather along the domain walls, and hence slow down the kinetics of the annealing process.

1. Introduction

The high-temperature superconducting material $YBa_2Cu_3O_{7-\delta}$, with an oxygen concentration ranging from $\delta = 1$ to $\delta = 0$, can be regarded as an interstitial solid solution of oxygen based on the tetragonal $YBa_2Cu_3O_6$ phase. A unit cell of $YBa_2Cu_3O_6$ is formed by three perovskite-type unit cells $a_0 \times a_0 \times c_0$ where $c_0 \sim 3a_0$, and a_0 is the perovskite lattice parameter. One perovskite unit cell $a_0 \times a_0 \times a_0$ gives rise to a plane of $CuO_{1-\delta}$ with Cu(1) atoms. These planes can easily be filled by oxygen atoms O(1) or O(5) which then sit on sites half the distance between nearest-neighbour Cu atoms. The oxygen atoms occupy these sites either at random, or along the x or y tetragonal axis, forming Cu–O–Cu chains and in this way causing a reduction of symmetry to orthorhombic symmetry, with an elongation of the lattice constant, either a or b respectively. Two other perovskite unit cells form CuO_2 planes (Cu(2) and O(2),O(3)) in which all oxygen sites are always occupied. These planes are commonly agreed to be responsible for superconductivity effects. The CuO_2 and $CuO_{1-\delta}$ layers are further bounded by apical oxygen (O(4)), which are located on the lines joining the Cu(1) and Cu(2) atoms.

At high temperatures a random distribution of oxygens in the $CuO_{1-\delta}$ plane gives the disordered tetragonal $YBa_2Cu_3O_{7-\delta}$ phase. At several hundred degrees centigrade the tetragonal $YBa_2Cu_3O_{7-\delta}$ crystal undergoes a ferroelastic and order–disorder phase transition to a low-temperature orthorhombic phase. This ordering results in a preferential oxygen occupation of one sublattice, either O(1) or O(5), in the $CuO_{1-\delta}$ plane. The T–δ temperature–oxygen-concentration phase diagram possesses several phases, which differ in oxygen arrangements within the $CuO_{1-\delta}$ planes (Krables *et al* 1991, Khachaturian and Morris 1988, Ceder *et al* 1990a, Ceder *et al* 1990b, de Fontaine *et al* 1990, Semenkovskaya and Khachaturian 1992). At elevated temperatures the oxygen concentration δ can be

0953-8984/94/010237+16$07.50

varied by changing the ambient oxygen pressure. At high oxygen concentrations, $\delta \sim 0$, the low-temperature orthorhombic OI structure consists of oxygen chains separated by one lattice constant. There are indications (Reyes-Gasga *et al* 1989, Yang *et al* 1992) that at intermediate concentrations, $\delta \sim 0.5$, the modulated OII structure appears with oxygen chains occupying every second oxygen sublattice. It is believed that all observed ordered structures differ only in the distribution of oxygens over the interstitial sites.

At room temperature the diffusion of oxygen atoms (Tsukui *et al* 1991) is so slow that a typical diffusion jump time is of the order of hours; therefore, the non-stoichiometric $YBa_2Cu_3O_{7-\delta}$ usually exists in the form of a stable or metastable coherent mixture of microdomains. Moreover, a slow diffusion of oxygen atoms at room temperature makes it difficult to determine the phase boundaries between the above-mentioned phases.

It has been established that the conducting carriers in the high-T_c superconducting cuprates have wavefunctions located mainly in the CuO_2 plane, and the relevant conduction states are $Cu{:}d_{x^2-y^2}$ and $O{:}p_\sigma$ (Furuyama 1991). It proves to be necessary to take into consideration the apical oxygens together with the $Cu{:}d_{z^2}$ orbitals of Cu(2). There are theoretical indications that the critical temperature is well correlated with the difference of the Madelung energies of apical O(4) and planar oxygens O(2) and O(3), and that the role of the apical oxygen atoms is to prescribe the stability of local singlet states made of two holes in the $Cu{:}d_{x^2-y^2}$ and $O{:}p_\sigma$ orbitals of the CuO_2 plane (Ohta *et al* 1991). On the other hand, a consideration of the four-bond model of $CuO_{1-\delta}$ chains together with upper and lower apical oxygens, made clear that the holes in the chains are delocalized and strongly correlated (Oleś and Grzelka 1991).

When the oxygen atoms enter the sublattices $CuO_{1-\delta}$, two effects compete: (i) the transfer of electrons from copper to oxygen atoms and (ii) the creation of conducting carriers (holes) in the CuO_2 plane through a charge transfer process (Jorgensen *et al* 1991). Hence, through the introduction of oxygen defects, the $YBa_2Cu_3O_{7-\delta}$ crystal becomes superconducting. A maximum of the transition temperature to the superconducting state is achieved for a non-stoichiometric oxygen concentration which involves a definite carrier concentration (Tallon *et al* 1991). However, as argued by Gupta and Gupta (1991) the charge transfer from the CuO_2 plane takes place only when the oxygen atoms of the $CuO_{1-\delta}$ planes are already ordered in chains. Burdett (1992) has argued that two effects, taking place in the $CuO_{1-\delta}$ plane, are responsible for the hole concentration in the CuO_2 plane. The first is related to the presence of isolated oxygen vacancies in the oxygen chains in an orthorhombic domain. Such vacancies lead to the generation of a hole excess in the band of Cu ions in the CuO_2 planes. This effect causes the 90 K plateau in the plot of the superconductivity transition temperature against oxygen concentration. The second effect is that short oxygen chains consisting of a few oxygen atoms are unable to transfer the charge from chains to the CuO_2 planes, since the energy levels generated by short chains lay above the Fermi level and are unable to accept electrons. This property is responsible for the 60 K plateau and the lack of superconductivity for an oxygen concentration below about $\delta = 0.62$. EPR studies on Gd^{3+} introduced to $YBa_2Cu_3O_{7-\delta}$ has shown (Pekker *et al* 1991) that the formation of chains begins at a threshold of oxygen content of $\delta = 0.86$.

The work by Jorgensen *et al* (1990) shows that the stoichiometry in oxygen alone is not a sufficient condition for the occurrence of superconductivity in $YBa_2Cu_3O_{7-\delta}$ and that the local ordering of oxygen atoms in chains of $CuO_{1-\delta}$ planes plays an equally important role. It has been shown that $YBa_2Cu_3O_{6.41}$ crystal quenched from 520°C into liquid nitrogen does not become superconducting down to 4.2 K. However, annealing the same sample at room temperature with no change of stoichiometry of oxygen results in a material which

is superconducting up to $\sim$ 20 K. This is of course a consequence of oxygen ordering in $CuO_{1-\delta}$ chains.

Another argument for the importance of oxygen ordering in superconductivity properties is the annealing experiment of Jorgensen *et al* (1991), in which the superconducting transition temperature of a $YBa_2Cu_3O_{6.45}$ single crystal was measured after quenching from 500°C and after subsequent annealing at room temperature for various periods of time. The transition temperature was 34 K immediately after quenching and increased with annealing time at room temperature to a maximum of 43 K after 167 hours. Moreover, neutron powder diffraction measurements have revealed that the average bond length between the copper atom Cu(2) and the apical oxygen atom O(4), decreased during annealing at room temperature by 0.6%.

Thus, in $YBa_2Cu_3O_{7-\delta}$ superconductivity is observed only in the orthorhombic phase. It is then tempting to speculate (Jorgensen *et al* 1991) that superconductivity disappears when the orthorhombic domain or the oxygen chain sizes fall below the superconducting planar coherence length, which in this material is of the order of $\sim$ 15 Å (Xu and Suenaga 1991). Indeed, every oxygen atom O(1) causes a small displacement of a neighbouring oxygen atom O(2) in the CuO_2 planes. This displacement does not occur when the oxygen site remains empty. When the domain is orthorhombic, the CuO_2 plane remains structurally coherent for superconductivity. When oxygen atoms are randomly distributed over O(1) sites, the structural coherence of CuO_2 is destroyed and the plane is tetragonal and may not become superconducting.

Further quenching and careful annealing experiments (Yang *et al* 1992) on $YBa_2Cu_3O_{7-\delta}$ with $\delta \sim 0.1$–0.5 performed at 51°C revealed two relaxation processes. The faster relaxation process is associated with changes in short-range oxygen order. The slower process, differing by two order of magnitudes compared to the faster process, is attributed to the restoration of long-range chains. It has been shown that the short-range disorder shortens the Cu–O chain segments and thus decreases the hole concentration and depresses the critical temperature of the superconducting state (Veal and Paulikas 1990).

The ordering of the oxygen atoms in the $CuO_{1-\delta}$ planes has already been studied within the framework of several models. The short-range asymmetric next-nearest neighbour Ising model (Ceder *et al* 1990a) has been used to investigate oxygen ordering in $CuO_{1-\delta}$ planes, and to calculate the temperature–oxygen-concentration phase diagram. The parameters of this model assume a repulsive interaction between the nearest and direct next-nearest oxygen atoms O–O, and an attractive interaction between those next nearest oxygen atoms O–Cu–O which are joined by a copper. The repulsive interaction comes from a Coulombic interaction between ions of the same kind. A Monte Carlo simulation of room-temperature aging showed that the time dependence of the population of four-coordinated Cu atoms can again be represented by two time constants, differing by almost a factor of 20 (Ceder *et al* 1990b, Ceder *et al* 1991). Unfortunately, this short-range interaction model of oxygen ordering cannot describe the tweed and polytweed patterns, whose appearance is related to the long-range strain-induced interaction.

The importance of a strain-induced interaction has been discussed in several papers. Marais *et al* (1991) have developed an Ising model with a strain-induced coupling; they showed by computer simulation that for some cases tweed microstructures, similar to tweed textures, evolve. Semenkovskaya and Khachaturyan (1992) have proposed a two-dimensional model describing oxygen ordering. The model includes both the long-range Coulomb-like repulsive interaction and the strain-induced interaction between ordered oxygen atoms. The model has been employed to investigate the kinetics of structural transitions using a computer simulation technique based on the crystal lattice-site diffusion

theory with the Landau–Ginzburg equation. Domains of a few orthorhombic structures have been found, and it has been shown that the transition path influences the structure of the ordered low-temperature phases.

Another two-dimensional displacive model of the $CuO_{1-\delta}$ plane, for the stoichiometric composition $\delta = 0$ (Parlinski *et al* 1993a), has been studied by the molecular–dynamics technique. In this model, the short-range oxygen–oxygen and copper–copper interactions are linearly coupled, leading to a long-range strain field. The system has a strong tendency to form a tweed structure, as observed experimentally. On quenching from high temperatures, a pronounced {1, 1} micro-twinning appears (Parlinski *et al* 1993b). Annealing at lower temperatures produces an intermediate stripe structure before annealing to a single domain. From the rate at which the distance between domain walls increases, a temperature–time–transition (TTT) diagram has been constructed, which shows strong similarities to those obtained from experiment.

In this paper we generalize the displacive model used previously (Parlinski *et al* 1993a), to the case of a non-stoichiometric oxygen concentration by adding to the potential energy an external field (chemical potential) coupled to the order parameter which measures the oxygen concentration. The molecular-dynamics technique is used to simulate the system. The temperature dependence of the order parameter which describes the tetragonal–orthorhombic phase transition allow us to determine the temperature–oxygen-concentration phase diagram. The transition temperature decreases quadratically with decreasing oxygen concentration. In the orthorhombic phase the strain fluctuations, being linearly coupled to the oxygen concentration field, form a grid of needle domains, and the density of these fluctuations increases with increasing degree of non-stoichiometry. On quenching to below the transition temperature, the texture first becomes more regular in spacing before the system orders macroscopically. The oxygen atoms try to avoid the domain boundaries, and therefore a higher concentration of oxygen vacancies is observed along the domain walls. This slows down the kinetic behaviour of the annealing process in the non-stoichiometric system.

2. Model

A two-dimensional model is proposed to simulate the behaviour of a single $CuO_{1-\delta}$ plane of the $YBa_2Cu_3O_{7-\delta}$ system. Each unit cell of the model crystallite has a square form and contains one copper atom at lattice site (i, j). There are two oxygen sites per unit cell, one lying halfway between copper atoms (i, j) and $(i + 1, j)$ on the X axis to be referred to as site 1, and with site 2 being halfway between copper atoms (i, j) and $(i, j + 1)$. The oxygen atoms are described by soft Ising variables $Z^{(1)}_{i,j}$ and $Z^{(2)}_{i,j}$, referring to sites 1 and 2 in cell (i, j), respectively. A positive value of $Z^{(k)}_{i,j}$ indicates the presence of an oxygen atom at site k in unit cell (i, j), while a negative value denotes a vacancy. The soft Ising variable is subject to the external field H, thus allowing one to change the concentration of oxygen atoms.

The potential energy V of the model is

$$V - Hx = V_{\text{elastic}} + V_{\text{intersite}} + V_{\text{local}} - V_{\text{external}} \tag{1}$$

where

$$V_{\text{elastic}} = \sum_{i,j} \left[A(R_{i,j;i+1,j} - a_0 - \alpha Z^{(1)}_{i,j})^2 + A(R_{i,j;i,j+1} - a_0 - \alpha Z^{(2)}_{i,j})^2 \right.$$
$$\left. + B(R_{i,j;i+1,j+1} - a_0\sqrt{2})^2 + B(R_{i,j;i+1,j-1} - a_0\sqrt{2})^2 \right] \tag{2}$$

$$V_{\text{intersite}} = \sum_{i,j} J\left[Z^{(1)}_{i,j} Z^{(2)}_{i+1,j} + Z^{(1)}_{i,j} Z^{(2)}_{i+1,j-1} + Z^{(2)}_{i,j} Z^{(1)}_{i,j} + Z^{(2)}_{i,j} Z^{(1)}_{i,j+1}\right] \tag{3}$$

$$V_{\text{local}} = \sum_{i,j} \left\{-E\left[(Z^{(1)}_{i,j})^2 + (Z^{(2)}_{i,j})^2\right] + G\left[(Z^{(1)}_{i,j})^4 + (Z^{(2)}_{i,j})^4\right]\right\} \tag{4}$$

$$V_{\text{external}} = \frac{1}{2} \sum_{i,j} H(Z^{(1)}_{i,j} + Z^{(2)}_{i,j}) \tag{5}$$

$$R_{i,j;i',j'} = \left[(X_{i,j} - X_{i',j'})^2 + (Y_{i,j} - Y_{i',j'})^2\right]^{1/2}. \tag{6}$$

Here, a_0 denotes the lattice constant and $(X_{i,j}, Y_{i,j})$ the position vector of the copper atom (i, j). Each copper atom is coupled to its nearest and next-nearest copper atoms by harmonic springs with spring constants A and B, respectively. This choice of forces guarantees that phonon normal modes form two acoustic branches, and hence the structure behaves correctly as an elastic medium. The interaction between oxygen atoms has two origins. Firstly, a direct coupling between oxygen atoms with positive coupling constant J, equation (3), follows from Coulomb repulsion. A positive value of J means that if one site is occupied then its nearest-neighbour sites are likely to be unoccupied. Secondly, $\alpha Z^{(1)}_{i,j}$ and $\alpha Z^{(2)}_{i,j}$ in the first two terms of (2), give a lengthening of the nearest-neighbour Cu–Cu distance when the intervening site is occupied, and a shortening when unoccupied. Such a local strain is propagated through the lattice by V_{elastic}.

The soft Ising variable is confined to the double well potential (4), with two parameters E and G. If the double well is very deep then the variable $Z^{(k)}_{i,j}$ is always near one of the minima, i.e. it behaves practically like an Ising variable $\sigma = \pm 1$. Denoting the occupancy of a site by an oxygen atom $\sigma = +1$ and a vacancy by $\sigma = -1$, the concentration deviation from a stoichiometric composition is given by the sum of σ over the whole system, normalized to the number of oxygen sites. By analogy, in a system with soft Ising variables we introduce the off-stoichiometry parameter

$$x = \frac{1}{2} \sum_{i,j} \left(\langle Z^{(1)}_{i,j} \rangle + \langle Z^{(2)}_{i,j} \rangle\right) \tag{7}$$

which is a measure of the oxygen concentration. To find the oxygen concentration itself, δ, we have to normalize x:

$$\delta = -\frac{x}{\sqrt{\langle Z^2 \rangle_0}} \tag{8}$$

where $\langle Z^2 \rangle_0 = E/2G$ is the mean square static displacement in the bare local double-well potential V_{local}, equation (4). Relation (8) follows from mean field theory and will be derived in the next section. Thus, varying the external field H, equation (5), one is able to modify the oxygen concentration, at least not very far from the stoichiometric value $x = 0.0$.

The numerical values of the potential parameters, $A = 2000$, $B = 8000$, $J = 2500$, $E = 3000$, $\alpha = 1.0$ and $G = 10^6$, have been chosen so that the ground-state configuration of the model has the required orthorhombic symmetry and the lattice deformation is about 6%. The model has been simulated using the molecular-dynamics technique (Parlinski 1987, 1988). The crystallite consisted of 99×99 unit cells with 29 205 particles. Free boundary conditions were used, with the edges of the crystallite cut along [1, 0] directions and consisting of copper. The free boundary conditions allowed the domain walls to flow in and out of the crystallite. The Newtonian equations of motion were solved iteratively by a simple

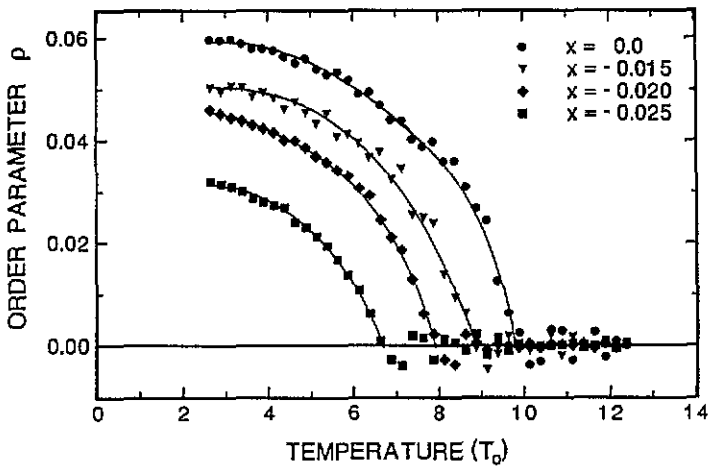

Figure 1. Strain order parameter as a function of temperature for several values of off-stoichiometry parameter x.

difference scheme with a time step $\Delta t = 0.002\tau_0$. A canonical ensemble, with constant temperature T and constant concentration x, was used. The temperature was defined by an average kinetic energy. The off-stoichiometry parameter x was kept constant by varying the magnitude of the external field H.

We have set the units of length to the lattice constant $a_0 = 1.0$, the particle mass $M_0 = 1.0$ and time unit $\tau_0 = 1.0$. Hence the energy and temperature units are $T_0 = M_0 a_0^2 \tau_0^{-2}$, the parameters A, B, J, E and G are in units of $M_0\tau_0^{-2}$ and $M_0\tau_0^{-2}a_0^{-2}$, respectively, and the external field H in units of $M_0\tau_0^{-2}a_0$.

3. Order parameter and phase diagram

The local strain coupled to oxygen–vacancy configurations can be deduced from the local-strain order parameter

$$\rho_{i,j} = \tfrac{1}{4}(\langle R_{i,j;i+1,j}\rangle + \langle R_{i,j;i-1,j}\rangle - \langle R_{i,j;i,j+1}\rangle - \langle R_{i,j;i,j-1}\rangle). \tag{9}$$

It is defined as the difference between the average distance of copper atoms in the X and Y directions around (i, j) lattice site. The $\rho_{i,j}$ is positive or negative when oxygen atoms form chains along the [1, 0] and [0, 1] directions, respectively. The sum

$$\rho = \frac{1}{N}\sum_{i,j}\rho_{i,j} \tag{10}$$

where N is the number of unit cells, determines the global strain order parameter of the ferroelastic tetragonal–orthorhombic phase transition; ρ decreases with increasing temperature and defines the transition temperature T_c^x when vanishing. To find T_c^x the system was heated for several values of x at a heat rate $\mathrm{d}T/\mathrm{d}t = 0.1$. This heat rate was slow enough to reach equilibrium at each temperature. Figure 1 shows the temperature dependence of the global strain order parameter for a few values of the off-stoichiometry parameter x. The temperature T_c^x decreases with decreasing oxygen concentration δ; T_c^x defines the phase boundary on the T–δ temperature–concentration phase diagram as shown in figure 2.

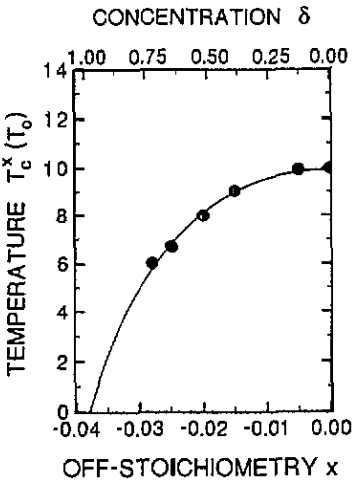

Figure 2. Calculated temperature–concentration-phase diagram showing the phase boundary between tetragonal and orthorhombic phases.

In the framework of mean field theory the phase boundary line can be derived with the aid of the Bogolyubov inequality for the free energy

$$g \leqslant g_0 + \langle V - V^\circ \rangle \tag{11}$$

where the brackets denote the thermodynamic average and g_0 is the value of the free energy of the local potential

$$V^\circ = \sum_{i,j} \{-E[(Z_{i,j}^{(1)})^2 + (Z_{i,j}^{(2)})^2] + G[(Z_{i,j}^{(1)})^4 + (Z_{i,j}^{(2)})^4] - \tfrac{1}{2}H(Z_{i,j}^{(1)} + Z_{i,j}^{(2)}) - (F_{i,j}^{(1)} Z_{i,j}^{(1)} + F_{i,j}^{(2)} Z_{i,j}^{(2)})\}. \tag{12}$$

The term V° represents the on-site potential with additional forces $F_{i,j}^{(1)}$ and $F_{i,j}^{(2)}$ which are used as variational parameters in accordance with the inequality (11). For simplicity, we ignore the role of V_{elastic} ($\alpha = 0$) in this process, so the $V - V^\circ$ potential energy becomes

$$V - V^\circ = \sum_{i,j} \{J[Z_{i,j}^{(1)} Z_{i+1,j}^{(2)} + Z_{i,j}^{(1)} Z_{i+1,j-1}^{(2)} + Z_{i,j}^{(2)} Z_{i,j}^{(1)} + Z_{i,j}^{(2)} Z_{i,j+1}^{(1)}] + (F_{i,j}^{(1)} Z_{i,j}^{(1)} + F_{i,j}^{(2)} Z_{i,j}^{(2)})\}. \tag{13}$$

The free energy g_0, corresponding to a single variable $Z_{i,j}^{(k)}$, where $k = 1, 2$, is

$$g_0(T, F) = -T \ln \int \mathrm{d}z \exp\left(\frac{-v(Z) - FZ}{T}\right) \tag{14}$$

where the indices have been suppressed and $v(Z) = EZ^2 + GZ^4 - \frac{1}{2}HZ$. Expanding over F, one finds

$$g_0(T, F) = g_0^\circ(T) - \langle Z \rangle_0 F - \frac{(\langle Z^2 \rangle_0 - \langle Z \rangle_0^2)}{2T} F^2 + \cdots \tag{15}$$

where

$$g_0^\circ(T) = -T \ln \int \mathrm{d}Z \exp\left(\frac{-v(Z)}{T}\right) \tag{16}$$

and the moments

$$\langle Z^l\rangle_0 = \int \mathrm{d}Z\, Z^l \exp\left(\frac{-v(Z)}{T}\right)\left[\int \mathrm{d}Z \exp\left(\frac{-v(Z)}{T}\right)\right]^{-1} \tag{17}$$

for $l = 1, 2$. The term $\langle Z\rangle_0$ denotes the shift of the mean displacement caused by the external field H, and $\langle Z^2\rangle_0$ is the mean square displacement calculated with the local potential only. Combining now (15) and (17) and minimizing with respect to $F_{i,j}^{(k)}$ in order to eliminate these forces, we find the approximate free energy to be

$$\begin{aligned} g = \sum_{i,j}\Bigg(2g_0^\circ(T) + 4Jx^2 + T\frac{\left(\langle Z_{i,j}^{(1)}\rangle - x\right)^2}{2\langle (Z^{(1)})^2\rangle_0} + T\frac{\left(\langle Z_{i,j}^{(2)}\rangle - x\right)^2}{2\langle (Z^{(2)})^2\rangle_0} \\ + J\left[\left(\langle Z_{i,j}^{(1)}\rangle - x\right)\left(\langle Z_{i+1,j}^{(2)}\rangle - x\right) + \left(\langle Z_{i,j}^{(1)}\rangle - x\right)\left(\langle Z_{i+1,j-1}^{(2)}\rangle - x\right)\right. \\ \left. + \left(\langle Z_{i,j}^{(2)}\rangle - x\right)\left(\langle Z_{i,j}^{(1)}\rangle - x\right) + \left(\langle Z_{i,j}^{(2)}\rangle - x\right)\left(\langle Z_{i,j+1}^{(1)}\rangle - x\right)\right]\Bigg). \end{aligned} \tag{18}$$

Here we have used the definition of x (equation (7)). Transforming the above free energy to reciprocal space, using

$$\langle Z_{i,j}^{(k)}\rangle - x = -(-1)^k \sum_{\boldsymbol{k}} Z(\boldsymbol{k}) \exp[2\pi \boldsymbol{k}\cdot(\boldsymbol{R}_{i,j}^\circ + \boldsymbol{r}_k)]$$

with $k = 1, 2$ and $\boldsymbol{r}_1 = (a_0/2, 0)$ and $\boldsymbol{r}_2 = (0, a_0/2)$, one finds

$$g = 2N[g_0^0(T) + 2Jx^2] + \frac{1}{2}\sum_{\boldsymbol{k}} \Omega(\boldsymbol{k}, T) Z(\boldsymbol{k}) Z(-\boldsymbol{k}) + \ldots \tag{19}$$

where

$$\Omega(\boldsymbol{k}, T) = \frac{T}{\langle Z^2\rangle_0 - x^2} + J(\boldsymbol{k}) \tag{20}$$

and

$$J(\boldsymbol{k}) = -2J[\cos\pi(k_x + k_y)a_0 + \cos\pi(k_x - k_y)a_0]. \tag{21}$$

We can now make an estimate of T_c^x defined at $\boldsymbol{k} = 0$ by the condition $\Omega(0, T_c^x) = 0$; it yields

$$T_c^x = 4J(\langle Z^2\rangle_0 - x^2). \tag{22}$$

For the order–disorder limit (Bruce 1980)

$$\langle Z^2\rangle_0 = \frac{E}{2G} = 0.0015 \tag{23}$$

which gives $T_c^{x=0} = 15.0T_0$, rather higher than the value $9.9T_0$ obtained for $x = 0$ from the simulation. This difference is due, at least in part, to our approximation of ignoring the strain system. Equation (22) describes the phase boundary on the temperature–concentration phase diagram. This parabolic shape fits the calculated points, provided the parameter J is taken as an effective $J_{\mathrm{eff}} = 1606$. The same equation can be used to establish the relationship between the concentration δ and the off-stoichiometry parameter x. Assuming a linear dependence, $\delta = -cx$, and noting that at $\delta = 1$ the critical temperature vanishes $T_c^{x_{\max}} = 0$, one finds from (22) and (23) that $\delta = -x/\sqrt{\langle Z^2\rangle_0} = -25.82x$.

4. Tweed microstructure

In order to show the tweed microstructure and fluctuations, it is convenient to draw shadowing maps of the local strain order parameter distribution of $\rho_{i,j}$, equation (9). As discussed in the previous paper (Parlinski *et al* 1993a) each of these order parameters varies between ± 0.0633, which become only occasionally slightly larger. Therefore, we take the range between -0.08 and $+0.08$, to which we assign shading from black to white, respectively. The data set $\{\rho_{i,j}\}$ at some typical instant of time were placed on a regular grid of 99×99 or 64×64 unit cells, and shading was assigned to each lattice site according to the amplitude $\rho_{i,j}$. The grid was not corrected for the lattice shear. Hence black and white regions correspond to two oppositely sheared orthorhombic domains, with gray lines being the domain walls.

In figure 3 we compare two maps of the strain order parameter distributions taken at the same reduced temperatures, $T = 0.74T_c^x$, and for two values of off-stoichiometry parameters, $x = 0.0$ and $x = -0.02$. The maps show that the nature of the disorder in the strain subsystem has the structure of needle-like microdomains running along $[1, \pm 1]$ directions. The needle-like shape is present both in the stoichiometric and in the non-stoichiometric crystals, although the density of fluctuations in the non-stoichiometric case are definitely higher, because the thermal fluctuations are additionally influenced by the potential field of the oxygen vacancies.

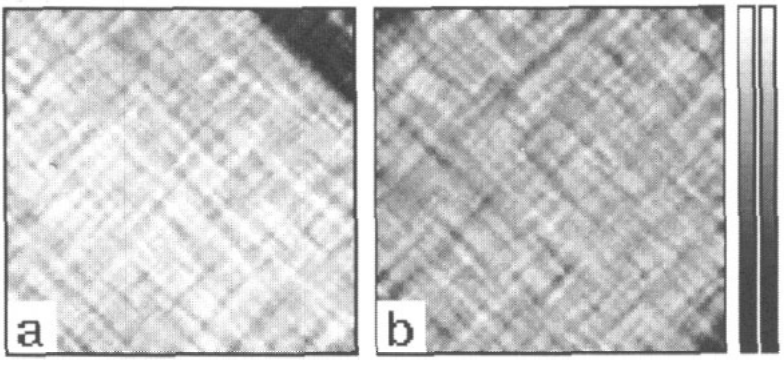

Figure 3. Comparison of two maps of the strain order parameter for off-stoichiometry parameters (*a*) $x = 0.0$ and (*b*) $x = -0.02$ at the same reduced temperature $T = 0.74T_c^x$. The maps show 99×99 unit cells.

The features of these fluctuations can be described by the correlation function $S(\boldsymbol{k})$ of the local-strain order parameter

$$S(\boldsymbol{k}) = \langle \rho^*(\boldsymbol{k}) \rho(\boldsymbol{k}) \rangle \tag{24}$$

where

$$\rho(\boldsymbol{k}) = \frac{1}{N} \sum_{i,j} \rho_{i,j} \exp(-2\pi \boldsymbol{k} \cdot \boldsymbol{R}^0_{i,j}) \tag{25}$$

and $\boldsymbol{R}^0_{i,j}$ denotes the position vector of the lattice point (i, j). To characterize the fluctuations one should concentrate on the $[1, \pm 1]$ directions. Thus, only the $S(q) = S(\boldsymbol{k})$ for

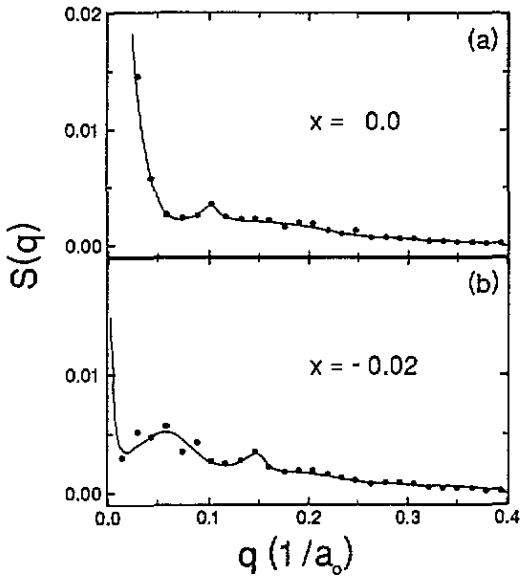

Figure 4. The correlation function $S(q)$ of the strain order parameter along the [1, 1] direction for two values of off-stoichiometry parameters (*a*) $x = 0.0$ and (*b*) $x = -0.02$ at the same reduced temperature $T = 0.74T_c^x$.

$\boldsymbol{k} = (q/\sqrt{2}, \pm q/\sqrt{2})$ lines have been calculated. Figure 4 shows the correlation function $S(q)$ for two values of the off-stoichiometry parameter, $x = 0.0$ and $x = -0.02$, and at the same reduced temperature, $T = 0.74T_c^x$.

Two characteristic length scales which describe the size of needle-like fluctuations are seen in the $S(q)$ functions. In the stoichiometric system the longitudinal and transversal sizes contribute to the maxima around $q = 0.0$ and $q = 0.1$, respectively. With increasing values of the off-stoichiometry parameter these contributions move towards higher wave vectors, showing that the sizes of fluctuations decrease.

To characterize the sizes of the fluctuations we have calculated the mean wave vector $\bar{q}$ of the $S(q)$ distributions

$$\bar{q} = \frac{S_1}{S_0} \tag{26}$$

with the aim of zeroth and first moments

$$S_0 = \int_{q_{\min}}^{q_{\max}} S(q)\,\mathrm{d}q \qquad S_1 = \int_{q_{\min}}^{q_{\max}} qS(q)\,\mathrm{d}q \tag{27}$$

where the intervals of the integrations have been chosen to be $q_{\min} = 0.01$ and $q_{\max} = 0.79$. The quantity reciprocal to $\bar{q}$ describes the mean size of fluctuations.

Figure 5 demonstrates changes in the mean wave vector $\bar{q}$ as a function of temperature for three values of off-stoichiometry parameter x. At the stoichiometric concentration $x = 0$, and when the temperature tends to zero, the amplitude of the fluctuations goes to zero, and therefore the mean wave vector $\bar{q}$ tends to zero as well. At a finite oxygen concentration the fluctuations survive down to the lowest temperatures and this effect is caused by the potential field of oxygen vacancies. The larger the off-stoichiometry, the higher the observed $\bar{q}$, and fluctuations of smaller sizes occur. At high temperatures in the tetragonal phase the size of fluctuations becomes independent of the oxygen concentration. In this region thermal fluctuations are so pronounced that the influence of oxygen vacancies and off-stoichiometry become marginal.

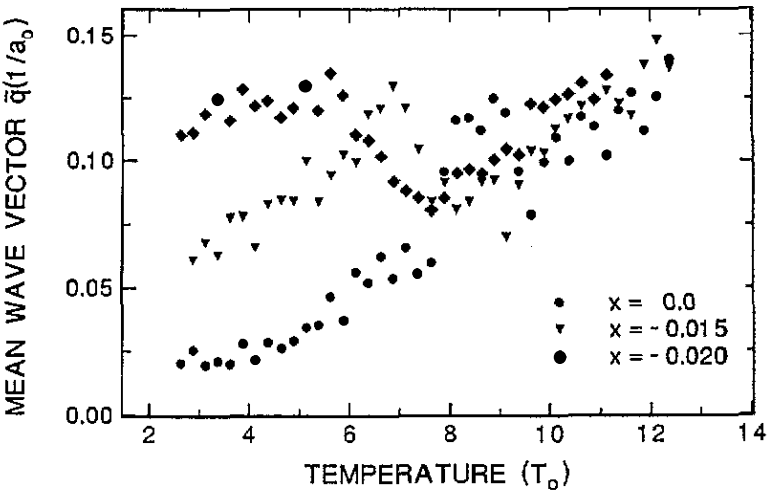

Figure 5. The mean wave vector $\bar{q}$ as a function of temperature calculated from the correlation function $S(q)$ of strain order parameter along [1, 1] direction for three values of off-stoichiometry parameters $x = 0.0, -0.015$ and -0.02.

5. Evolution of the tweed microstructure

The evolution of the tweed microstructure depends upon many factors, particularly time, quench and annealing temperature T_a. Here we study such an evolution during the following process. The initially equilibrated system in the tetragonal phase was quenched to the annealing temperature. This was achieved by the fast reduction of particle velocities. After the quench, isothermal conditions were applied and the system was left to relax towards equilibrium. During this process the formation and time evolution of the microstructure was studied.

The results of three typical runs with off-stoichiometry parameters $x = 0.0, -0.015$ and -0.025 initially quenched from $T = 1.24T_c^x$ to $T_a = 0.63T_c^x$, the same in reduced temperature units for each value of x, are shown on the maps of the strain order parameter in figure 6. The degree of undercooling below T_c^x is rather large, therefore the domain walls are narrow and the thermodynamic drive towards equilibrium is strong. The first snapshots of figure 6(*a*), (*e*), (*i*) taken after the short annealing time of $0.3\tau_0$ show a definite, although very fine, tweed microstructure, which seems to be independent on the off-stoichiometry parameter x. In the course of time, the number of right-angle domain wall junctions reduces rapidly, indicating that junction energies are high and prohibit wall crossing. After a long annealing time all domain walls should disappear. This seems to be the case for stoichiometric oxygen concentration, figure 6(*d*), where a large area of single orthorhombic domains has already been built up. However, for non-stoichiometric concentration the stripe pattern persists much longer, since, as observed in figure 7, the oxygen vacancies gather along the domain walls. In figure 7 the map of the strain order parameter is compared with the map of the soft Ising variables $\eta_{i,j}$, defined as a symmetric form of the off-stoichiometry parameter distribution, equation (7)

$$\eta_{i,j} = \tfrac{1}{4}\big(\langle Z^{(1)}_{i,j}\rangle + \langle Z^{(1)}_{i-1,j}\rangle + \langle Z^{(2)}_{i,j}\rangle + \langle Z^{(2)}_{i,j-1}\rangle\big). \tag{28}$$

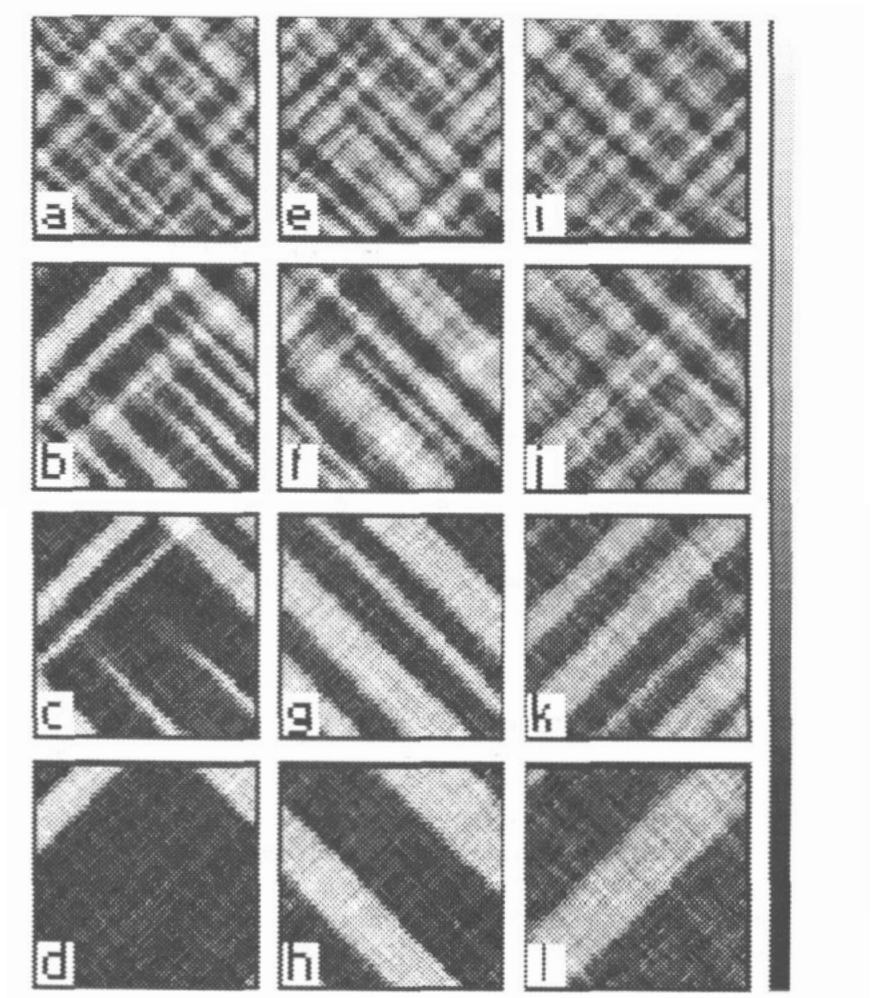

Figure 6. Maps of the strain order parameter obtained during annealing at temperature $T_a = 0.63T_c^x$ after quenching from temperature $T = 1.24T_c^x$, for three values of off-stoichiometry parameters (*a*)–(*d*) $x = 0.0$, (*e*)–(*h*) $x = -0.015$, (*i*)–(*j*) $x = -0.025$. Maps (*a*), (*e*), (*i*); (*b*), (*f*), (*j*); (*c*), (*g*), (*k*); and (*d*), (*h*), (*l*) correspond to annealing time $t = 0.3, 0.9, 3.0$ and $20.0\tau_0$, respectively. The maps show 99×99 unit cells.

The shading gradation from black to white denotes the vacancies and oxygen atoms, respectively. Both maps have been taken for the same region of the crystallite and at the same time. Map figure 7(*b*) illustrates the distribution of oxygen atoms, and indicates clearly that oxygen vacancies prefer to reside at the domain walls. A similar conclusion has been reached from the electron energy loss spectroscopy measurements (Blais *et al* 1991) made on $YBa_2Cu_3O_{7-\delta}$. There, the oxygen concentration was systematically lower in the twin boundaries than in the domain of the crystal. Our simulation results indicate that the oxygen vacancies hinder the motion and hence delay the annihilation of the domain walls.

Our model supports the observation that the oxygen vacancies, which normally stay in oxygen chains, accumulate on the coherent domain wall. Indeed, at the domain wall directed along [1, 1] or [1, −1] the neighbouring oxygen atoms, belonging to two opposite orthorhombic domains, also belong to the two different sublattices $Z^{(1)}$ and $Z^{(2)}$. These

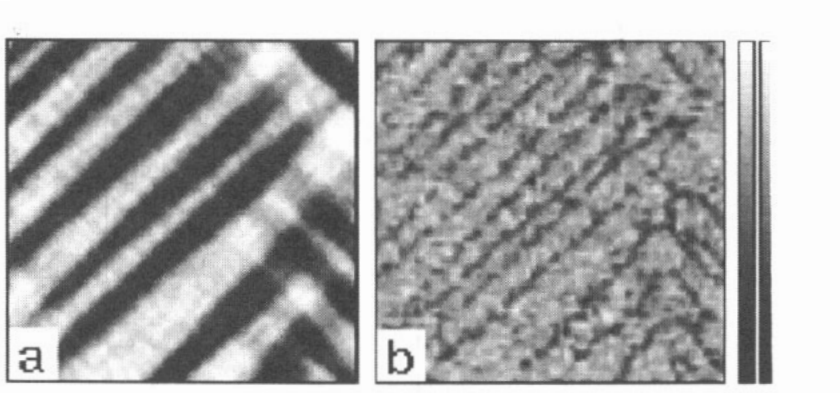

Figure 7. Comparison of (*a*) the map of strain order parameter with (*b*) the map indicating the oxygen concentration distribution for $x = -0.015$ and temperature $T = 0.22T_c^x$. The maps show 64 × 64 unit cells.

two oxygen sites interact via the antiferro-coupling, equation (3), therefore they increase locally the potential energy. This energy can, however, be lowered if an oxygen vacancy moves from the bulk to the domain wall. Indeed, from (4), one can estimate the energy of the oxygen vacancy in the bulk and on the domain wall to be $8JZ_0^2$ and $2JZ_0^2$ respectively, and $J > 0$.

Figure 6 shows that the length scales of the tweed and stripe patterns increase with increasing time, and this process is usually referred to as coarsening. Our rather small system is too small for a satisfactory deduction of the relevant rate laws. Nevertheless, we have calculated the correlation function $S(q)$ along the [1, 1] or [1, −1] directions perpendicular to stripes to characterize the time evolution of the microstructure. Figure 8 shows a number of $S(q)$ calculated for three values of off-stoichiometry parameters $x = 0.0, -0.015, -0.025$, which correspond to the maps shown in figure 6. The characteristic wall–wall distances appear as maxima in the correlation functions. At the early stage of coarsening the maxima occur around $q = 0.05, 0.08$ and 0.09, respectively. With increasing time the distribution functions become narrower and shift to lower wave vector. To describe the average sizes of domains we have again followed the experimental procedure expressed by (26) and (27), which define the characteristic mean wave vector $\bar{q}$. The results for the correlation function $S(q)$ are shown in figure 9. At the beginning of the annealing process a gradual decrease of $\bar{q}$ is observed, approximately the same for each concentration. However, after a period of about $2\tau_0$ the process became more rapid for the stoichiometric system $x = 0$, leading eventually at $4\tau_0$ to a structure with a predominant single domain. In non-stoichiometric systems the domain sizes do not grow so rapidly, and even at $20\tau_0$ a stripe pattern is still observed. Later stages of coarsening are inaccessible by our simulation, since separation between domain walls becomes of the same order of magnitude as the size of the simulated crystallite.

6. Concluding remarks

We have shown that a remarkably simple model can demonstrate a rich microstructure of tweed texture, the coarsening of the tweed annealing to a single domain through an intermediate stripe phase for both the stoichiometric and non-stoichiometric oxygen concentrations. It was not necessary to complicate the model by considering oxygen atoms

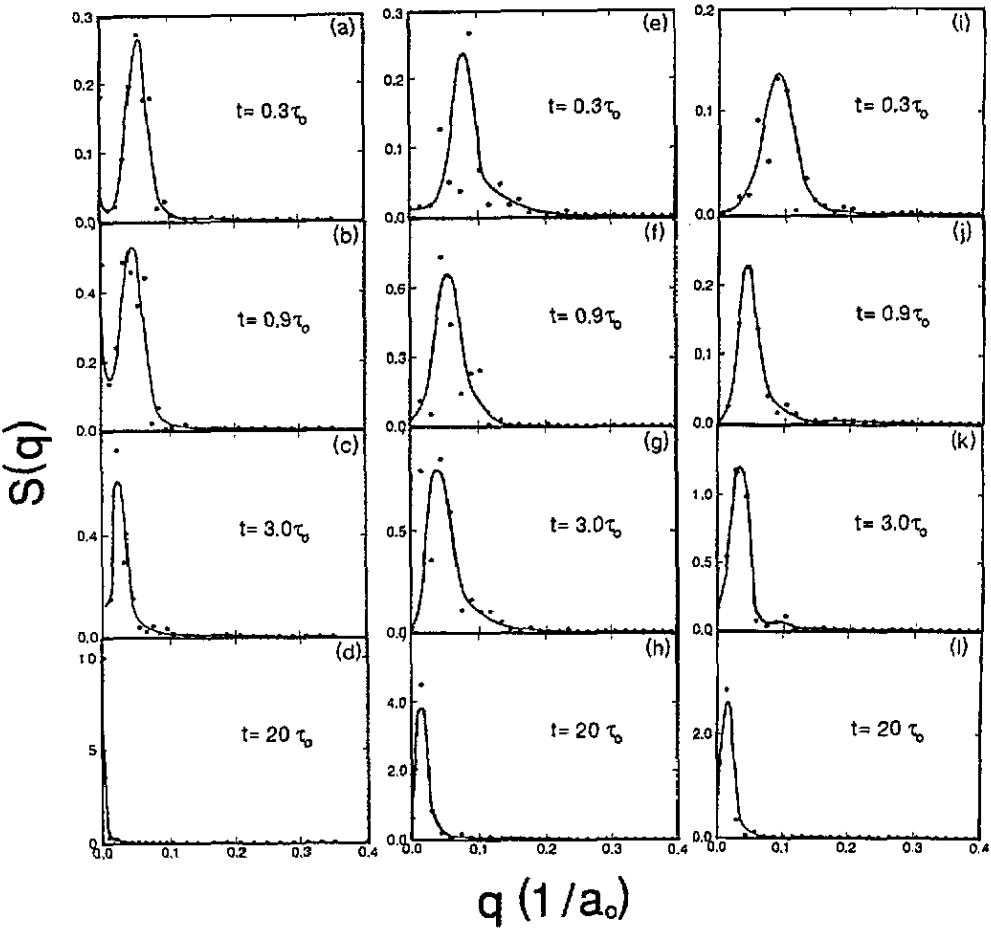

Figure 8. The correlation functions $S(q)$ of the strain order parameter as a function of wave vector q in $[1, 1]$ for (a)–(d) and (i)–(l) and in $[1, -1]$ for (e)–(h) directions and at the annealing temperature $T_a = 0.63T_c^x$. $S(q)$ has been calculated during the same process as the maps of figure 6.

as part of the elastic medium. It was sufficient to take account that when the oxygen site is occupied by an oxygen atom it pushes the adjacent copper atoms apart, whereas when the site is empty the copper atoms are pulled together somewhat. The domain boundaries cost a lot of strain energy unless they lie along the $[1, \pm 1]$ directions. Hence, any fluctuations tend to form needles.

Our model is an extension of an earlier one (Parlinski *et al* 1993) which was confined to stoichiometric material $\delta = 0$. Here we have supplemented the local potential energy by a term with an external field and related it to the oxygen concentration by the mean displacements. There are practical advantages to this method. This approach avoids to the explicit consideration of oxygen diffusion, thus from the algorithmic point of view the table of neighbours is fixed and the calculations are much less time consuming. Moreover, the continuous variables still allow us to treat the system by molecular dynamics. Otherwise one would have to treat it in a mixed way, Monte Carlo sampling for the discrete σ variables and molecular dynamics for the $X_{i,j}, Y_{i,j}$ continuous variables, which is more cumbersome

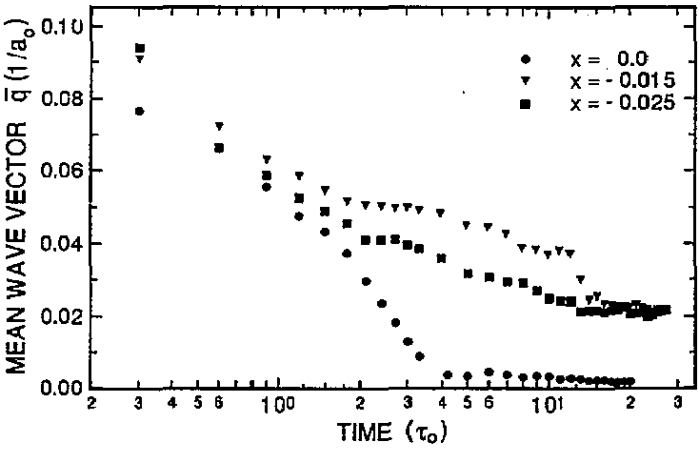

Figure 9. Mean wave vector $\bar{q}$, equation (26), which characterizes the average linear size of domains in $[1, \pm 1]$ directions as a function of logarithm of annealing time at $T = 0.63T_c^x$ for three values of off-stoichiometry parameters.

and again more time consuming. Thus, the prize to be paid for the above-mentioned simplifications is that our description of the concentration of oxygen atoms is approximate but this, as we have seen, does not change the qualitative behaviour of the system.

This model is unable to reproduce the modulated phases OII and OIII in which every second or third oxygen chain, respectively, remains empty. The reason for that is the oversimplified direct interaction between oxygen atoms, which takes into account only the potential energy between the nearest oxygen neighbours. To stabilize any of the modulated phases an interaction at least up to next-nearest neighbours would be needed.

Acknowledgments

The authors wish to thank A M Oleś for fruitful discussions. The work has been fully supported by the State Committee of Scientific Research (KBN), grant No 2 2377 92 03.

References

Blais S, Thomas O, Sénateur J-P, Weiss F and Audieu M 1991 *Physica* C **185–9** 545
Bruce A D 1980 *Adv. Phys.* **1** 111
Burdett J 1992 *Physica* C **191** 282
Ceder G, Asta M, Carter W C, Kraitchman M and de Fontaine D 1990a *Phys. Rev.* B **41** 8698
Ceder G, Asta and de Fontaine D 1990b *Physica* C **177** 106
Ceder G, McCormack R and de Fontaine D 1991 *Phys. Rev.* B **44** 2377
de Fontaine D, Ceder G and Asta 1990 *Nature* **343** 544
—— 1990 *J. Less-Common Met.* **164–5** 108
Furuyama H 1991 *Physica* C **185–9** xxv
Gupta M and Gupta R P 1991 *Physica* C **185–9** 851
—— 1991 *Phys. Rev.* B **44** 2739
Jorgensen J D, Shiyou Pei, Lightfoot P, Hao Shi, Paulikas A P and Veal B W 1990 *Physica* C **167** 571
Jorgensen J D, Hinks D G, Radaelli P G, Shiyou Pei, Lightfoot P, Dabrowski B, Segre C U and Hunter B A 1991 *Physica* C **185–9** 184

Khachaturyan A G and Morris J W Jr 1988 *Phys. Rev. Lett.* **61** 215
Krables G, Bieger W, Wieser U, Ritchel M, Hauk J and Altenburg H 1991 *Physica* C **185–9** 503
Marais S, Heine V, Nex C and Salje E 1991 *Phys. Rev. Lett.* **66** 2480
Ohta Y, Tohyama T and Maekaw S 1991 *Phys. Rev. Lett.* **66** 1228
—— 1991 *Phys. Rev.* **43** 2968
Oleś A M, Grzelka W 1991 *Phys. Rev.* B **44** 9531
Parlinski K 1987 *Phys. Rev.* B **35** 8690
—— 1988 *Comput. Phys. Rep.* B **8** 153
Parlinski K, Heine V and Salje E K H 1993a *J. Phys.: Condens. Matter* **5** 497
Parlinski K, Salje E K H and Heine V 1993b *Acta Metall.* A **41** 839
Pekker S, Jánossy A and Rockenbauer A 1991 *Physica* C **181** 11
Reyes-Gasga J, Krekels T, Van Tendeloo G, Van Landuyt J, Amelinckx S, Bruggink W H M and Werweij H 1989 *Physica* C **159** 831
Semenkovskaya S and Khachaturiyan A G 1992 *Phys. Rev.* B **46** 6511
Tallon J L, Buckley R G, Haines E M, Presland M R, Mawdsley A, Flower N E and Loran J 1991 *Physica* C **185–9** 855
Tsuki S, Yamamoto T, Adachi M, Shono Y, Kawabata K, Fukuoka N, Yanase A and Yoshioka Y 1991 *Physica* C **185–9** 929
Veal B W, You H, Paulikas A P, Shi H, Fang Y and Downey J W 1990 *Phys. Rev.* B **42** 4770
Xu Y and Suenaga M 1991 *Phys. Rev.* B **43** 5516
Yang S, Claus H, Veal B W, Wheeler R, Paulikas A P and Downey J W 1992 *Physica* C **193** 243